ResearchGate

See discussions, stats, and author profiles for this publication at: https://www.researchgate.net/publication/24042498

Computer Simulation of Volatile Organic Compound Adsorption in Atomistic Models of Molecularly Imprinted Polymers

ARTICLE *in* LANGMUIR · MARCH 2009

Impact Factor: 4.46 · DOI: 10.1021/la804168b · Source: PubMed

CITATIONS
37

READS
42

2 AUTHORS, INCLUDING:

Lev Sarkisov
The University of Edinburgh
61 PUBLICATIONS **1,634** CITATIONS

SEE PROFILE

Available from: Lev Sarkisov
Retrieved on: 04 February 2016

Langmuir Article

pubs.acs.org/Langmuir
© 2009 American Chemical Society

Computer Simulation of Volatile Organic Compound Adsorption in Atomistic Models of Molecularly Imprinted Polymers

Carmelo Herdes and Lev Sarkisov*

Institute for Materials and Processes, University of Edinburgh, EH9 3JL United Kingdom

Received December 18, 2008. Revised Manuscript Received February 3, 2009

Molecularly imprinted polymers (MIPs) offer a unique opportunity to significantly advance volatile organic compound (VOC) sensing technologies and a number of other applications. However, the development of these applications using MIPs has been hindered by poor understanding of the microstructure of MIPs, geometry of binding sites, and the details of molecular recognition processes in these materials. This is further complicated by the vast number of optimization parameters such as building components and processing conditions. Computer simulations and molecular modeling can help us understand adsorption and binding phenomena in MIPs on the molecular level and thus provide a route to more efficient MIP design strategies. So far, molecular models have been either oversimplified or severely limited in length scale, essentially focusing on a single binding site. Here, we propose a more general, atomistically detailed model that describes the microstructure of MIPs. We apply this model to investigate adsorption of pyridine, benzene, and toluene in MIPs and demonstrate that it is able to capture a number of essential experimental features. Therefore, this model can serve as a starting point in computational design and optimization of MIPs.

I. Introduction

Molecularly imprinted polymers (MIPs) have been playing an increasingly important role in volatile organic compound (VOC) sensing for air quality control, explosives and warfare agent detection, and other important applications. The unique feature of these materials is their biomimetic molecular recognition functionality, that is, their ability to detect and strongly bind specific molecules from an array of analogues in a preprogrammed fashion.

This molecular recognition functionality is achieved via a synthesis protocol known as imprinting of polymers. The principles of this technique are schematically shown in Figure 1. The prepolymerization mixture consists of cross-linker, functional monomer, template, and solvent species. Template molecules form transient associations with the functional monomers, and this stage of the synthesis is usually called the complexation step. This is followed by polymerization, with the cross-linker providing the rigidity and integrity of the structure. Removal of the template and solvent leaves cavities in the structure with the shape and interaction patterns complementary to the template molecules. Hence, we obtain a MIP which is able to recognize and rebind the original template species. A number of MIPs have been proposed over the years for chromatographic separations, artificial immunoassays, drug delivery, and other applications.[1−3] Sensing applications of MIPs have been recently reviewed by Blanco-Lopez et al.[4] and by McCluskey et al.[5] Recently, Fu and Finklea proposed a series of MIPs for quatrz crystal microbalance (QCM) sensor to detect toluene, benzene, and other VOCs.[6] In their study, the proposed polymers were based on ethylene glycol dimethacrylate (EGDMA) as the cross-linker, methacrylic acid (MAA) as the functional monomer, and either hydroquinone or phenol as the template. Among several interesting results, they successfully demonstrated that a sufficient level of sensitivity can be obtained using the proposed MIPs, with toluene adsorbing stronger than benzene and MIPs exhibiting binding constants several times higher than those for nonimprinted control polymers. In another interesting example, Bunte and co-workers recently proposed several materials based on EGDMA and a range of functional monomers for 2,4,6-trinitrotoluene (TNT) gas phase sensing.[7]

Despite these successes, several challenges exist in rational design of new MIPs with specific functionalities for sensing. It has been well established in a number of studies that MIPs have few selective binding sites and a large number of relatively nonselective sites.[2,8] This heterogeneity of binding sites is both an intrinsic and unavoidable feature of the imprinting technique. High quality, very specific binding sites form as a result of associations between the functional monomers and template species. Thus, most of the recent design efforts have been focused on screening for appropriate functional monomers, which would form strong complexes with the template molecule of interest. At the same time, systematic structural characterization of MIPs has been rather limited. Physisorption of nitrogen is one of the techniques traditionally used to obtain structural characteristics of porous solids. Analysis of nitrogen adsorption isotherms using the well-known methods, such as Brunauer−Emmett−Teller

*To whom correspondence should be addressed. E-mail: Lev.Sarkisov@ed.ac.uk.

(1) Mayes, A. G.; Whitcombe, M. J. *Adv. Drug Delivery Rev.* **2005**, *57*, 1742.

(2) Spivak, D. A. *Adv. Drug Delivery Rev.* **2005**, *57*, 1779.

(3) Alexander, C.; Andersson, H. S.; Andersson, L. I.; Ansell, R. J.; Kirsch, N.; Nicholls, I. A.; O'Mahony, J.; Whitcombe, M. J. *J. Mol. Recognit.* **2006**, *19*, 106.

(4) Blanco-Lopez, M. C.; Lobo-Castanon, M. J.; Miranda-Ordieres, A. J.; Tunon-Blanco, P. *Trends Anal. Chem.* **2004**, *23*, 36.

(5) McCluskey, A.; Holdsworth, C. I.; Bowyer, M. C. *Org. Biomol. Chem.* **2007**, *5*, 3233.

(6) Fu, Y.; Finklea, H. O. *Anal. Chem.* **2003**, *75*, 5387.

(7) Bunte, G.; Hurttlen, J.; Pontius, H.; Hartlieb, K.; Krause, H. *Anal. Chim. Acta* **2007**, *591*, 49.

(8) Umpleby, R. J.; Baxter, S. C.; Rampey, A. M.; Rushton, G. T.; Chen, Y. Z.; Shimizu, K. D. *J. Chromatogr., B* **2004**, *804*, 141.

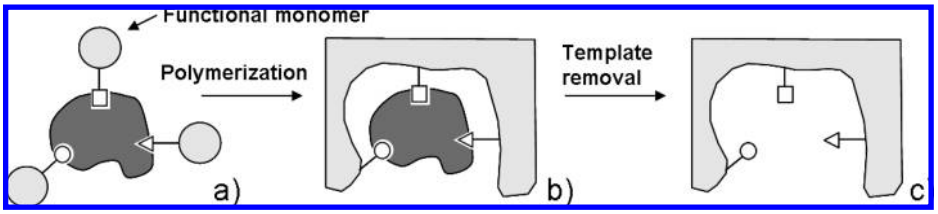

Figure 1. Schematic depiction of polymer imprinting principles. The first stage (on the left) involves complexation between functional monomers (shown in light gray) and the template (shown in dark gray). This is followed by polymerization (shown in the center) and template removal, leading to the cavity shown on the right. This cavity serves as a binding site to recognize and bind molecules structurally similar to the template.

(BET) and Barrett−Joiner−Halenda (BJH), generates information about the surface area and pore size distribution in a porous solid.[9] These methods have been recently applied to several families of MIP materials.[10,11] It has been shown that many MIPs feature the surface area in the range between 40 and 436 m^2/g and pore sizes in tens of nanometers range. Little, however, is known about the structure of MIPs in the microporous range (<2 nm). This is associated with several factors. In order to assess microporosity of materials, nitrogen adsorption measurements must be conducted at very low pressures ($10^{-7}-10^{-2} p/p_0$), and this presents a technical difficulty for most of the standard adsorption rigs. Even when these measurements are possible, analysis of the data is not straightforward, as a number of assumptions involved in, for example, the BJH analysis fail in the microporous regime. Most importantly, although a large variety of MIPs has been synthesized over the years, accurate analysis of their structure with respect to microporosity has been simply neglected.

Although it is estimated that the volume of micropores in a typical MIP is not exceeding about 5% of the total pore volume, structural characterization of microporosity of MIPs is important. First, the imprinted binding cavities have dimensions of a single molecule, that is, several angstroms, and thus, a single binding site could be viewed as a micropore. Second, in many applications, such as VOC sensing, adsorption processes take place at very low pressures of the adsorbate, not exceeding few mbars and typically less than 1 mbar. In this pressure range, adsorption takes place in micropores, and rational design of new MIPs for sensing applications requires a detailed description of this process. However, currently our understanding of the microstructure of MIPs, the geometry of the binding sites, and the nature of molecular recognition in these sites is very fragmented.

We believe molecular simulations can fundamentally advance our ability to design and synthesize new MIPs. First and foremost, molecular simulations provide a unique insight into the system on a detailed atomistic level and therefore are able to explain and elucidate microscopic behavior. Furthermore, these studies may suggest new strategies and new protocols for design of materials with specific functions. Finally, molecular simulations, if brought to a sufficient level of accuracy, can be used as a cost-effective tool in material design optimization by being able to scan through several building components and processing conditions.

A number of fundamental models of MIPs have been recently proposed.[12−22] For example, Yungerman and Srebnik have recently considered a model of a polymerizing Lennard−Jones fluid templated with rigid dimers, also made of two Lennard−Jones sites.[20] Polymerization was modeled as formation of harmonic bonds between the particles representing monomers. This model allowed the authors to investigate porosity and pore size distribution in the final structure as function of the template concentration and degree of polymerization. Wu et al. recently proposed a simple 2D square lattice model of MIPs.[22] In the model, each lattice site can be either empty or occupied by a cross-linker, functional monomer, or template particle. Each functional monomer can form an association with only one out of four adjacent lattice sites. The template site can have up to four monomers associated with it. This leads to binding sites of different types and quality (depending on the number of monomers associated with the site). This model is clearly well suited to explore binding site distributions in MIPs and how this characteristic depends on the relative concentrations of the template and monomer species and on the strength of the template-functional monomer association. However, molecular recognition emerges as a result of shape complementarity between the molecule and the binding site. Lattice description lacks molecular structure detail, and thus, this model cannot be used to study recognition phenomena, except for a special case of racemic systems. Van Tassel and co-workers have recently proposed a series of off-lattice models featuring rigid molecular species.[12−15,19,21] Their models, studied within the framework of integral equation theories and in computer simulations, exhibited a number of interesting effects, including some elements of molecular recognition. However, these models have so far been confined to some simplified description of the MIP components.

More detailed atomistic simulations have been also employed to study MIPs. Computational design of MIPs has been proposed by Piletsky and co-workers, based on

(9) Rouquerol, J.; Rouquerol, F.; Sing, K. S. W. *Absorption by Powders and Porous Solids*; Academic Press: New York, **1999**.
(10) Al Kobaisi, M.; Tate, M.; Rix, C.; Jakubov, T. S.; Mainwaring, D. E. *Adsorption* **2007**, *13*, 315.
(11) Urraca, J. L.; Carbajo, M. C.; Torralvo, M. J.; Gonzalez-Vazquez, J.; Orellana, G.; Moreno-Bondi, M. C. *Biosens. Bioelectron.* **2008**, *24*, 155.
(12) Van Tassel, P. R. *Phys. Rev. E* **1999**, *60*, R25.
(13) Zhang, L. H.; Van Tassel, P. R. *Mol. Phys.* **2000**, *98*, 1521.
(14) Zhang, L. H.; Van Tassel, P. R. *J. Chem. Phys.* **2000**, *112*, 3006.
(15) Cheng, S.; Van Tassel, P. R. *J. Chem. Phys.* **2001**, *114*, 4974.
(16) Zhang, L. H.; Cheng, S. Y.; Van Tassel, P. R. *Phys. Rev. E* **2001**, *64*, 042101.
(17) Srebnik, S.; Lev, O. *J. Chem. Phys.* **2002**, *116*, 1096.
(18) Srebnik, S. *Chem. Mater.* **2004**, *16*, 883.
(19) Sarkisov, L.; Van Tassel, P. R. *J. Chem. Phys.* **2005**, *123*, 164706.
(20) Yungerman, I.; Srebnik, S. *Chem. Mater.* **2006**, *18*, 657.
(21) Sarkisov, L.; Van Tassel, P. R. *J. Phys. Chem. C* **2007**, *111*, 15726.
(22) Wu, X. Y.; Carroll, W. R.; Shimizu, K. D. *Chem. Mater.* **2008**, *20*, 4335.

the energy minimization methods to quantify interactions between various monomers and imprint molecules.[23−25] For example, these calculations were used as a screening tool to select monomers for polymer synthesis, and, in particular, the best monomers were identified for complexation with creatine, ephedrine, and microcystin-LR.[23] Pavel and Lagowski applied molecular dynamics methods to calculate interaction energies in different monomer-imprint mixtures and also extended this approach to small polymerized clusters as model porous materials.[26−28] Monti et al. developed a computational approach based on a combination of molecular dynamics, molecular mechanics, and binding protocols to investigate the formation of possible imprinted structures in the presence of theophylline.[29] Although some interesting insights have been gained, most of these efforts suffer from two major drawbacks. The first drawback is the focus on binding within a single cavity. Issues related to the heterogeneity of binding sites, binding phenomena over a range of concentration regimes, and accessibility of pore space thus remain beyond the scope of these models. The second drawback of these models is that material optimization is reduced to a simplified scoring function approach based on the internal energy of complexation, rather than on proper adsorption isotherms (or, if the process takes place in solution, rebinding isotherms) as measured in experiments.

Here, we aim to develop a more general model of MIPs with a specific emphasis on sensing applications. The model, on one side, should feature a sufficient level of realism and detail, specifically be based on accurate force fields, and reflect some basic principles behind MIP formation and function. At the same time, it should operate on long enough length scales to capture the complex porous morphology of MIPs. Thiswill allow us to explore the relation between MIP porosity, pore size distribution, binding site heterogeneity, and binding functionality of these structures within the framework of one model. Predictions of this model, such as adsorption isotherms, can be directly compared to the experimental data.

In this study, we focus on a specific MIP based on methacrylic acid (MAA) as the functional monomer, ethylene glycol dimethacrylate as the cross-linker, and chloroform as the solvent. This system has been widely explored in experiments (although not necessarily in the context of sensing applications), it features relatively simple species, and it therefore provides a suitable starting point for the atomistic simulation studies. The system is templated with pyridine, which is also the simplest template possible and has been investigated in earlier studies.[30] We investigate adsorption of pyridine in templated and nontemplated model materials. Furthermore, we investigate adsorption of VOC molecules, toluene and benzene, in model MIP structures. The idea is to test whether the model is able to recognize pyridine among these similar species and to explore the theoretical sensitivity range of these materials toward pyridine and VOCs. Furthermore, another test of the model is its ability to exhibit preferential adsorption of toluene over benzene as has been observed experimentally in similar systems.[6] Finally, we explore how these properties depend on the porosity (degree of polymerization) of the system and the ratio of template to functional monomer concentrations in the polymerization mixture.

II. Methodology

II.1. General Computational Strategy. The idea of the strategy adopted here is to reflect the actual process of MIP formation. Thus, the first stage of our model involves mixing and equilibration of the required components in the specified proportions. The equilibration of the system takes place under typical experimental conditions. This is followed by quenching of the system (i.e., molecules are frozen in their instant locations). This step imitates polymerization, as the model at this stage does not explicitly describe formation of new chemical bonds. This is followed by the removal of the template and solvent species from the system. The resulting rigid structure of functional monomer and cross-linker serves as a model porous matrix in the consequent adsorption studies. In order to capture different degrees of cross-linking, we manipulate porosity of the system simply by varying the amount of solvent present in the prepolymerization mixture.

II.2. Molecular Models. Molecular species involved in this study are methacrylic acid (MAA), ethylene glycol dimethacrylate (EGDMA), chloroform ($CHCl_3$), pyridine (PYR), benzene (BEN), and toluene (TOL). To describe interactions among these species we adopt the TraPPe force field.[31−39] Specifically, this force field provides interaction parameters for benzene and toluene.[34] TraPPE parameters for pyridine and chloroform have been developed by Rai and Siepmann[39] and by Kamath et al.,[40] respectively.

Thus, the remaining species are MAA and EGDMA. To the best of our knowledge, there is no reported molecular simulation study focused specifically on MAA. Recently, Kamath and co-workers[41] and Clifford and co-workers[42] proposed TraPPe-like models of saturated carboxylic acids. We adopt parameters proposed by Clifford and co-workers to describe the carboxyl group of the MAA molecule, while the rest of the molecule is described via the available TraPPe parameters. In order to validate the model, we employ the Gibbs ensemble Monte Carlo (GEMC[43]) method to investigate MAA vapor−liquid equilibrium (VLE) phase behavior.

The basic details of the Gibbs ensemble simulation are as follows. The system consists of two simulation boxes, which are allowed to exchange molecules and change their size. The total volume of the system and the total number of the molecules remain constant, and therefore, the simulation is performed in the *NVT* ensemble. As the simulation progresses, one box

(23) Chianella, I.; Lotierzo, M.; Piletsky, S. A.; Tothill, I. E.; Chen, B. N.; Karim, K.; Turner, A. P. F. *Anal. Chem.* **2002**, *74*, 1288.
(24) Karim, K.; Breton, F.; Rouillon, R.; Piletska, E. V.; Guerreiro, A.; Chianella, I.; Piletsky, S. A. *Adv. Drug Delivery Rev.* **2005**, *57*, 1795.
(25) Chianella, I.; Karim, K.; Piletska, E. V.; Preston, C.; Piletsky, S. A. *Anal. Chim. Acta* **2006**, *559*, 73.
(26) Pavel, D.; Lagowski, J. *Polymer* **2005**, *46*, 7528.
(27) Pavel, D.; Lagowski, J. *Polymer* **2005**, *46*, 7543.
(28) Pavel, D.; Lagowski, J.; Lepage, C. J. *Polymer* **2006**, *47*, 8389.
(29) Monti, S.; Cappelli, C.; Bronco, S.; Giusti, P.; Ciardelli, G. *Biosens. Bioelectron.* **2006**, *22*, 153.
(30) Andersson, H. S.; Koch-Schmidt, A. C.; Ohlson, S.; Mosbach, K. *J. Mol. Recognit.* **1996**, *9*, 675.
(31) Martin, M. G.; Siepmann, J. I. *J. Phys. Chem. B* **1998**, *102*, 2569.
(32) Chen, B.; Siepmann, J. I. *J. Phys. Chem. B* **1999**, *103*, 5370.
(33) Martin, M. G.; Siepmann, J. I. *J. Phys. Chem. B* **1999**, *103*, 4508.
(34) Wick, C. D.; Martin, M. G.; Siepmann, J. I. *J. Phys. Chem. B* **2000**, *104*, 8008.
(35) Chen, B.; Potoff, J. J.; Siepmann, J. I. *J. Phys. Chem. B* **2001**, *105*, 3093.
(36) Stubbs, J. M.; Potoff, J. J.; Siepmann, J. I. *J. Phys. Chem. B* **2004**, *108*, 17596.
(37) Lubna, N.; Kamath, G.; Potoff, J. J.; Rai, N.; Siepmann, J. I. *J. Phys. Chem. B* **2005**, *109*, 24100.
(38) Wick, C. D.; Stubbs, J. M.; Rai, N.; Siepmann, J. I. *J. Phys. Chem. B* **2005**, *109*, 18974.
(39) Rai, N.; Siepmann, J. I. *J. Phys. Chem. B* **2007**, *111*, 10790.
(40) Kamath, G.; Georgiev, G.; Potoff, J. J. *J. Phys. Chem. B* **2005**, *109*, 19463.
(41) Kamath, G.; Cao, F.; Potoff, J. J. *J. Phys. Chem. B* **2004**, *108*, 14130.
(42) Clifford, S.; Bolton, K.; Ramjugernath, D. *J. Phys. Chem. B* **2006**, *110*, 21938.
(43) Panagiotopoulos, A. Z. *Mol. Phys.* **1987**, *61*, 813.

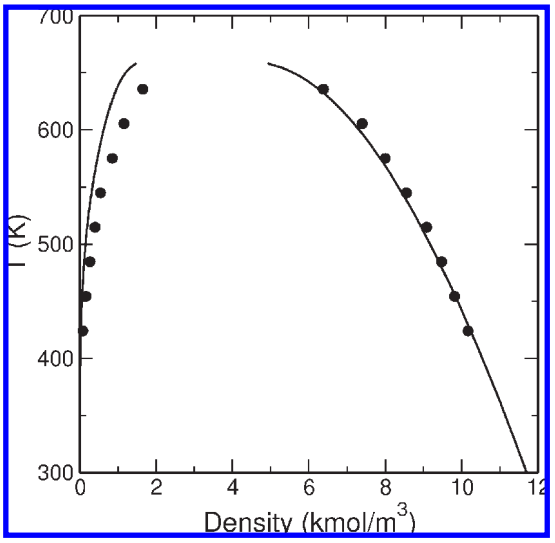

Figure 2. Temperature (K) versus density (kmol/m^3) vapor−liquid coexistence curves for bulk methacrylic acid (MAA) from the Gibbs ensemble computer simulations (●) and the reference experimental data (lines).[44]

evolves toward the liquid phase whereas the other one evolves toward the coexisting vapor phase. Hence, the properties of the phases in coexistence are calculated directly in a single simulation. The calculated interactions include Lennard−Jones interactions with the standard Lorentz−Berthelot mixing rules applied to the interactions between united atoms of different types and long-range electrostatic contributions, calculated using the Ewald summation. We consider 300 MAA molecules in the system. Increasing the number of molecules does not significantly alter the results presented here. Equilibration of the system, as evidenced from the averages of vapor and liquid densities, is achieved within 5×10^6 Monte Carlo (MC) steps. The production periods during which the equilibrium data is recorded involve between 3×10^6 and 6×10^6 MC steps. In order to improve sampling efficiency of the simulation, we implement the configurational bias Monte Carlo (CBMC) as described by Martin and Siepmann.[33] Thus, configurations of the system are sampled by volume change (0.006), configurational bias insertion and deletion of the molecules (0.196), molecule regrowth (0.267), translation (0.266), and rotation (0.267), with the relative weights of the attempted moves given in the brackets. Other details of the simulations are provided in the Supporting Information. The simulated VLE results for MAA can be seen in Figure 2. Good agreement with the available experimental data[44] is observed, particularly with regard to the saturated liquid densities (mean absolute errors are less than 1.1%). Although options do exist for improving the vapor density prediction, the goal of this model is to accurately represent the saturated liquid densities, which are more relevant for the density of MIPs.

EGDMA is a diester formed by condensation of two equivalents of MAA and one equivalent of ethylene glycol. Therefore, we model the EGDMA molecule with two MAA units, as described above, and one bridging ethylene glycol, following the work of Stubbs et al. on ethers, glycols, ketones, and aldehydes.[36] In the absence of extensive experimental data on EGDMA, in order to probe the molecular model, we perform a short (about 100 ps) molecular dynamics simulation of a small sample of EGDMA at $p = 1$ atm and $T = 298$ K. Pressure and temperature are maintained via the Berendsen baro- and thermostat.[45] The system contains 100 EGDMA molecules. The average density of the system is about 1102 kg/m^3, which compares reasonably well with the properties of EGDMA at similar conditions (1051 kg/m^3 at $T = 298$ K as supplied by Sigma-Aldrich).

A sensitive test of the accuracy of the adopted molecular force field is its ability to reproduce association constants between functional monomers and templates. From the spectroscopic measurements, the association constants of MAA with several templates are in the range between 3 and 30 M^{-1} or less, depending on the template.[46] We perform a molecular dynamics simulation of a mixture of MAA, pyridine, and chloroform at $p = 1$ atm and $T = 298$ K and monitor the number of hydrogen bonds formed between the carboxyl group of MAA and nitrogen of pyridine. The association constant estimated from this calculation is in the range between 1.5 and 3 M^{-1} (a more careful estimation can be made with a larger system and longer runs).

Species involved in MIP formation (MAA, EGDMA, chloroform, and pyridine) are shown in TraPPe representation in Figure 3 (the sizes of the interaction sites do not correspond to the actual collision diameters; here, we focus simply on the number and types of interaction sites involved in the description of each component).

II.3. Simulation Details. To synthesize a MIP, one starts with mixing the required components in the appropriate solvent. In the proposed model, we mimic this step by equilibrating a mixture of MAA, EGDMA, chloroform, and pyridine at the specified pressure and temperature. This is implemented via molecular dynamics simulations in the *NpT* ensemble. The number of molecules depends on the material under study. The pressure, p, is set to 1 bar and the temperature, T, to 300 K. With the time step of 0.002 ps and at least 15×10^6 time steps for each run, the simulations sample at least 30 ns. Periodic boundary conditions are used for the simulation boxes. The LINCS algorithm is employed to constrain the molecular bonds, and the Berendsen coupling scheme is adopted for baro- and thermostat;[45] the particle mesh Ewald (PME) method is used for electrostatic calculations.[47,48] Nonbonded interactions are cut off and shifted at 10 Å. All molecular dynamics simulations are performed using the Gromacs simulation package.[49,50] To visualize and to analyze the results of the simulations, we use the visual molecular dynamics (VMD) software.[51] The snapshot in Figure 4a, shows a typical equilibrated mixture of 40 pyridine (blue and yellow), 40 methacrylic acid (red), 200 EGDMA (gray), and 50 chloroform (green) molecules. The system is about 3.8 nm by 4.0 nm by 5.0 nm in size.

In experiments, the next step involves polymerization of the cross-linker and functional monomer, followed by the template and solvent removal. In the proposed model, we imitate this step by quenching molecules in their instant locations and by removing the template and solvent components. The snapshot in Figure 4b shows the same system as in Figure 4a with chloroform and pyridine molecules removed and the remaining species quenched.

The resulting structure serves as a model MIP for the consequent adsorption studies. The GCMC simulations of adsorption are performed using the multipurpose simulation code MuSiC.[52] In adsorption studies, all adsorbate species (pyridine, toluene, benzene) are considered as rigid molecules.

(44) DIPPR (Design Institute for Physical Properties) Database, DIADEM, 2004.
(45) Berendsen, H. J. C.; Postma, J. P. M.; Vangunsteren, W. F.; Dinola, A.; Haak, J. R. *J. Chem. Phys.* **1984**, *81*, 3684.
(46) Sellergren, B.; Lepistoe, M.; Mosbach, K. *J. Am. Chem. Soc.* **1988**, *110*, 5853.
(47) Darden, T.; York, D.; Pedersen, L. *J. Chem. Phys.* **1993**, *98*, 10089.
(48) Essmann, U.; Perera, L.; Berkowitz, M. L.; Darden, T.; Lee, H.; Pedersen, L. G. *J. Chem. Phys.* **1995**, *103*, 8577.
(49) Lindahl, E.; Hess, B.; van der Spoel, D. *J. Mol. Model.* **2001**, *7*, 306.
(50) Van der Spoel, D.; Lindahl, E.; Hess, B.; Groenhof, G.; Mark, A. E.; Berendsen, H. J. C. *J. Comput. Chem.* **2005**, *26*, 1701.
(51) Humphrey, W.; Dalke, A.; Schulten, K. *J. Mol. Graphics* **1996**, *14*, 33.
(52) Gupta, A.; Chempath, S.; Sanborn, M. J.; Clark, L. A.; Snurr, R. Q. *Mol. Simul.* **2003**, *29*, 29.

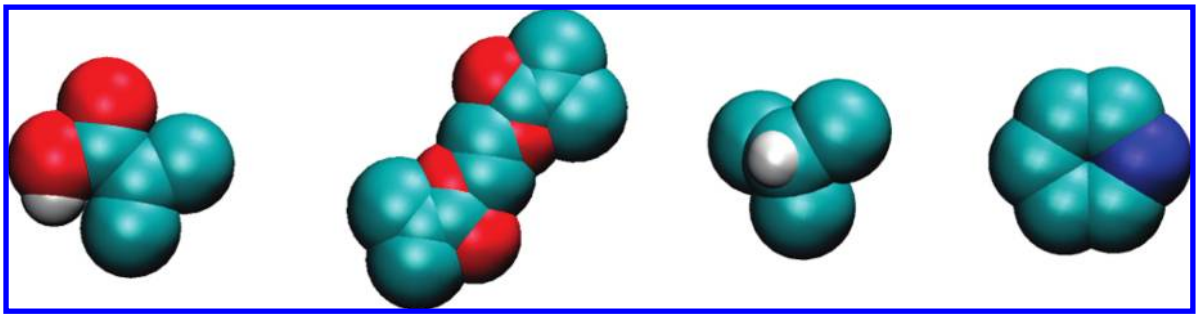

Figure 3. Molecular visualization of the components involved in the model. From left to right, molecules of MAA, EGDMA, chloroform, and pyridine are shown, with carbon groups shown in cyan, oxygen in red, nitrogen in dark blue, and atomistic hydrogen in gray. In this figure, the sizes of the interaction sites do not correspond precisely to the proper collision diameters (σ) of these sites in the simulation; the figure serves for illustration only.

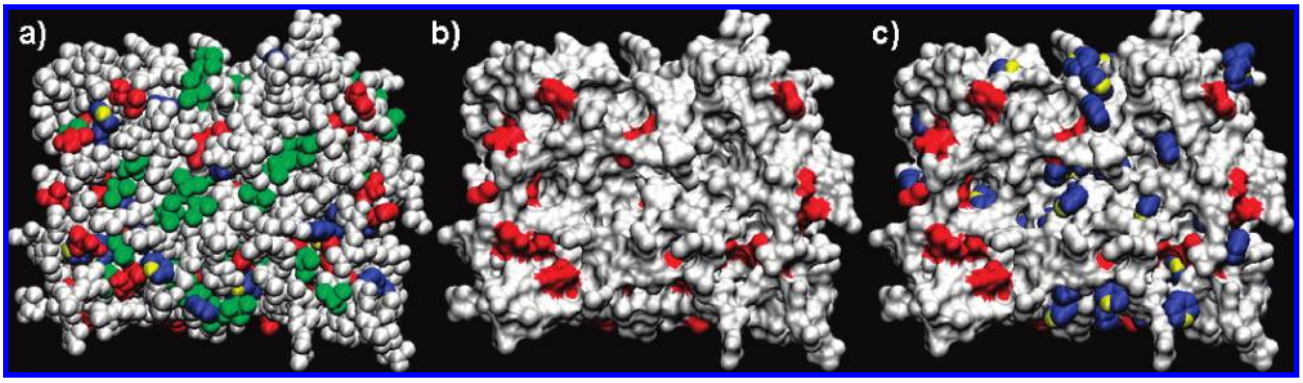

Figure 4. Computer graphics visualizations of the various stages of MIP4:4_d material formation and function. The visualization on the left shows a snapshot of the final configuration of an equilibrium mixture of methacrylic acid MAA (red), ethylene glycol dimethacrylate EGDMA (gray), chloroform $CHCl_3$ (green), and pyridine PYR (blue with the amino group shown in yellow). The visualization in the middle shows the same configuration with the solvent ($CHCl_3$) and template (PYR) removed. This configuration is used as model matrix for adsorption simulation, with the visualization on the right showing pyridine molecules adsorbed in the MIP4:4_d matrix at $p/p_0 = 0.98$.

To improve the efficiency of sampling, we implement the energy biased grand canonical Monte Carlo (EB-GCMC) protocol proposed in application to zeolites by Snurr and co-workers.[53] Therefore, the sampling protocol includes four types of moves, specifically biased insertions and deletions, random rotations, and translations with equal distribution of weights among the moves. For each adsorption point, 20×10^6 GCMC steps (each step being an attempt either to insert, delete, rotate, or translate a molecule) are performed, with half of the steps taken to equilibrate the system and the other half to sample the data. We model several materials with different porosities, which are described in more detail in the next section. For each material, we consider only a single matrix realization. A more thorough analysis should include averaging the data over several matrix realizations; however, this protocol is computationally intensive. (For the longest runs, formation of the system takes about 96 CPU hours on a single AMD Opteron 880/8218 processor and the complete adsorption/desorption isotherm takes about 72 h on a single processor of this type). We perform realization sensitivity analysis for selected systems only and observe that the qualitative outcomes presented in this article are valid for other realizations. Adsorption data are presented as the excess fluid density adsorbed in a MIP versus either absolute pressure p or relative pressure p/p_0 of the bulk phase; here, p_0 is the bulk saturation pressure for each pure fluid. Fugacities of the species at particular bulk pressures are calculated using the Peng−Robinson equation of state. The snapshot on the right in Figure 4c shows a typical configuration of pyridine adsorbed in a model MIP matrix (the snapshot corresponds to about 30 pyridine molecules adsorbed at $p/p_0 = 0.98$).

III. Results

We prepared a total of nine MIP materials, and their characteristics are summarized in Table 1. The MIP1:4 family features 10 pyridine, 40 MAA, and 200 EGDMA molecules, thus giving a typical experimental 1:4:20 proportion of the template, functional monomer, and cross-linker components, respectively. For the MIP4:4 family, this proportion is 4:4:20, with a total of 40 pyridine molecules considered in the system. These two families of materials are contrasted with a group of nonimprinted materials, NIP, with the proportion of the components being 0:4:20. During the equilibration process, we observe formation of transient complexes between pyridine and MAA. However, this process is significantly disturbed by the propensity of MAA to form dimers. (These dimers were also observed in experimental studies of MAA in bulk solutions[54].) On the other hand, pyridine features only one functional group, and since the complex can form with only one MAA molecule, the complex is relatively weak as suggested in previous experimental studies.[30] In our model, the porosity of materials is controlled by the amount of solvent present in the system. This is analogous to the experiments, where solvent occupies space that becomes pores

(53) Snurr, R. Q.; Bell, A. T.; Theodorou, D. N. *J. Phys. Chem.* **1993**, *97*, 13742.

(54) Buback, M.; Mahling, F. O. *J. Supercrit. Fluids* **1995**, *8*, 119.

Table 1. Summary of the Compositions and Characteristics (Surface S, m^2/g, and pore Volume V, cm^3/g) of the Systems (See Details in the Text)

materials		PYR	MAA	EGDMA	$CHCl_3$	S (m^2/g)	V (cm^3/g)
NIP	a	0	40	200	760	2836	1.648
	b				380	2144	0.872
	c				190	1235	0.467
	d				50	217	0.142
MIP1:4	a	10	40	200	760	2511	1.685
	b				380	1870	0.899
	c				190	1053	0.483
	d				50	279	0.175
MIP4:4	a	40	40	200	760	2729	1.744
	b				380	2205	0.982
	c				190	1410	0.564
	d				50	592	0.251

after polymerization and solvent removal. As we do not have an explicit mechanism of polymerization, in this model, different porosities of the prepared materials can be viewed as different degrees of cross-linking, with the denser materials corresponding to the higher degrees of cross-linking. Our initial intent was to optimize the amount of chloroform so that the resulting model structure reproduces experimental nitrogen adsorption isotherm in the low pressure region. Unfortunately, lack of the data in that region makes accurate fitting impossible, and therefore, we focus on a *range* of plausible structures. For each family of materials, we consider four compositions (series *a*, *b*, *c*, and *d*) ranging from 760 chloroform molecules (series *a*) to 50 (series *d*). For each material, we calculate accessible surface area, pore volume, and pore size distribution, using a range of computational tools employed earlier.[55−57] The amount of chloroform has a dramatic effect on the structural characteristics of the materials. At the highest concentration of solvent, these materials exhibit surface areas up to 2836 m^2/g and porosities about 1.7 cm^3/g. As we decrease the amount of chloroform, the surface areas and porosities decrease substantially. For example, with 50 chloroform molecules, MIP1:4_d has the surface area of 279 m^2/g (which compares well with the typical experimental values[10]) and porosity of 0.175 cm^3/g. It is also important to note that MIP and NIP counterparts (for example, NIP_c vs MIP1:4_c, or MIP4:4_c) have similar surface areas, with the exception of MIP4:4_d. Thus, just like in experiments, MIP and NIP structures cannot be distinguished based on this parameter. As we decrease the amount of solvent, we also start to observe a growing impact of the template presence. Specifically, at the lowest concentration of the solvent (series *d*), imprinted materials have significantly enhanced surface area and porosity, compared to the nonimprinted material, and this effect is particularly strong for MIP4:4_d system. Interestingly, all nine structures considered here are microporous. The top graph in Figure 5 compares pore size distributions calculated for MIP4:4_a and MIP4:4_d. As is evident from Table 1, MIP4:4_a has the highest porosity (the lowest density) out of nine materials. However, the largest pore size present in the structure is about 14 Å, with the majority of pores being around 10 Å in size. The lower graph in Figure 5 compares pore size distributions in NIP_d (nonimprinted) material and MIP4:4_d. Although the porosity of MIP4:4_d is significantly higher than that for NIP_d, the effect of imprinting is less evident from the pore size distribution.

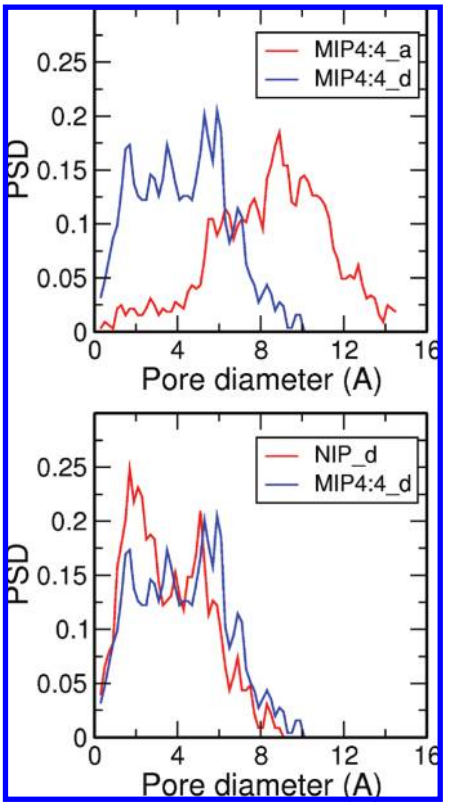

Figure 5. Pore size distribution (PSD) as a function of pore diameter (Å). Top graph examines the effect of polymer density (solvent concentration) and compares a low density MIP4:4_a polymer (red line) with a higher density MIP4:4_d polymer (blue line). Lower graph explores the effect of templating and compares the PSD for a nonimprinted polymer NIP_d (red line) and an imprinted polymer MIP4:4_d (blue line).

Next, we perform pure component adsorption simulations of pyridine, toluene, and benzene in the model materials. All nine structures exhibit preferential adsorption of pyridine over toluene and benzene, and preferential adsorption of toluene over benzene. Figure 6 compares adsorption isotherms for the most porous family of materials (series *a*, with top graphs a, b, and c corresponding to NIP_a, MIP1:4_a, and MIP4:4_a, respectively) and the least porous family of materials (series *d*, with the bottom graphs a, b, and c corresponding to NIP_d, MIP1:4_d, and MIP4:4_d, respectively). The top graphs represent only a portion of the complete isotherms, with a focus on the same pressure range as for the bottom graphs. Complete adsorption isotherms are available in the Supporting Information. It is clear from the figure that, for very porous materials (which can be viewed as materials with a low degree of cross-linking), the presence of the template has a negligible effect on the adsorption properties of the structure. Preferential adsorption of pyridine over toluene is associated simply with a stronger interaction of pyridine with available carboxyl groups due to the presence of the amino group. Compared to benzene, interaction of toluene with a MIP has an additional Lennard−Jones contribution from the methyl group.

(55) Gelb, L. D.; Gubbins, K. E. *Langmuir* **1998**, *14*, 2097.
(56) Gelb, L. D.; Gubbins, K. E. *Langmuir* **1999**, *15*, 305.
(57) Duren, T.; Sarkisov, L.; Yaghi, O. M.; Snurr, R. Q. *Langmuir* **2004**, *20*, 2683.

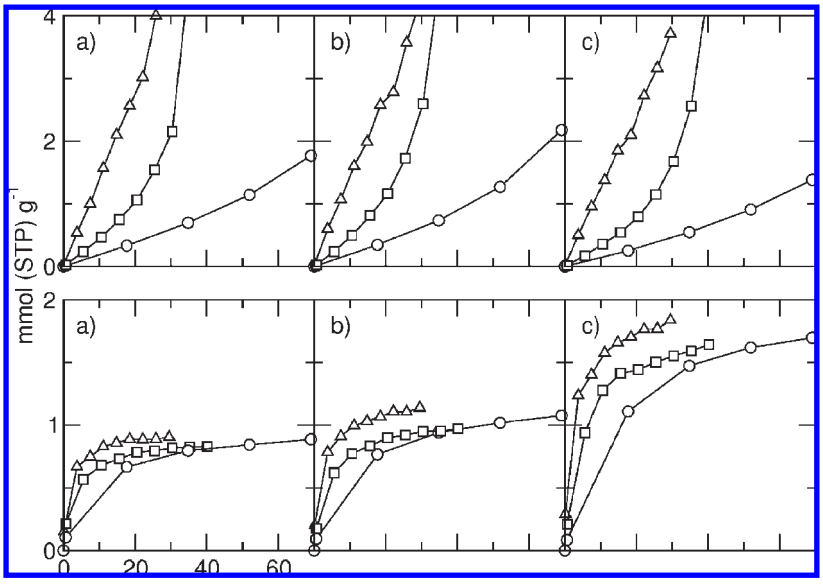

Figure 6. Adsorption isotherms at $T = 300$ K for benzene (○), toluene (□), and pyridine (△). The top graphs correspond to the most porous series *a* of materials, with graphs a, b, and c corresponding to NIP_a, MIP1:4_a, and MIP4:4_a, respectively. The lower graphs correspond to the least porous series of materials *d*, with graphs a, b, and c corresponding to NIP_d, MIP1:4_d, and MIP4:4_d, respectively. The isotherms are plotted as excess density mmol (STP)/g versus pressure *p* (mbar). The pressure scale is provided for the lower left graph and is the same all the graphs in the figure.

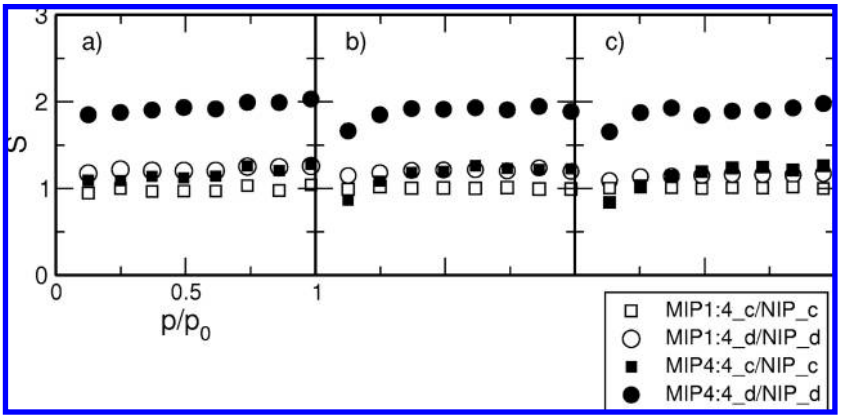

Figure 7. Ratio of adsorbed densities for pyridine (a), toluene (b), and benzene (c) in the imprinted materials and the corresponding nonimprinted analogues as a function of the relative pressure p/p_0. Squares correspond to MIP1:4_c/NIP_c (□) and MIP4:4_c/NIP_c (■); circles correspond to MIP1:4_d/NIP_d (○) and MIP4:4_d/NIP_d (●).

Although this contribution is not as strong as the hydrogen bond interaction between methacrylic acid and pyridine, it leads to preferential adsorption of toluene over benzene. This is in qualitative agreement with the recent experimental studies on similar MIPs (where phenol was employed as the template).[6] Similar trends are observed for much denser structures (Figure 6, bottom graphs). However, the shape of the isotherms is notably different, exhibiting signs of saturation in the same pressure range. This is clearly due to much lower porosity in these materials. One can describe these adsorption isotherms using the IUPAC classification.[9] In analogy to other studies of disordered porous materials and model slit pores, as the size of pores is systematically reduced, we observe a shift from type V (or type IV) isotherm, characteristic for mesoporous materials, to type I isotherm, describing microporous filling. (In the Supporting Information file, we also show that the isotherms for series *a* materials exhibit hysteresis characteristic for type IV and V isotherms). The effect of the template is also much more pronounced for denser structures, leading to higher loadings in the imprinted materials compared to the nonimprinted material NIP_d. In Figure 7, we plot the ratio of adsorbed density of pyridine in the imprinted materials and the corresponding density in the nonimprinted counterparts. There is a particularly significant enhancement of pyridine adsorption in MIP4:4_d material compared to NIP_d. Similar trends are observed for other materials and other adsorbates (in Figure 7, graphs b and c correspond to toluene and benzene, respectively). The enhancement of adsorption in the imprinted materials over the nonimprinted counterparts for toluene and benzene is comparable with that observed in experiments.[6] Interestingly, in our study, this enhancement has very similar values for all three adsorbates (about 2 for MIP4:4_d). It seems that the primary role of pyridine as template is to enhance porosity of the imprinted materials compared to the nonimprinted ones. As the sizes of all three adsorbates are similar, the effects of higher porosity are also similar. Moreover, a stronger degree of confinement in series *d*

of materials does not lead to the exclusion or diminished adsorption of toluene, which is a bulkier molecule than benzene.

IV. Discussion

We have presented a detailed atomistic model of microporous MIP materials. In the IIntroduction, we argued that a desirable model of MIPs should be based on accurate interactions between the components, it should reflect the essential elements of the synthetic protocol, it should operate on a sufficient length scale (beyond a single binding cavity), and it should be able to reproduce some experimental results. Remarkably, these objectives are met in the current model, although it is still oversimplified. It is based on the force fields validated using the vapor−liquid phase equilibria of individual components. Assembly of the model imitates the actual process of MIP synthesis. The model captures the structure of MIPs on the scale of a few nanometers. The model captures adsorption of VOCs and the effect of templating in qualitative agreement with the experiments (unfortunately, a direct comparison with the experiments is not possible at this stage, as the experimental data for the VOCs of interest are not available in the form of complete adsorption isotherms). Most importantly, this model offers a unique opportunity to visualize the realistic microstructure of MIPs and to link the features of this structure to adsorption and molecular recognition properties of the model material.

It is also important to identify the scope and the limitations of the model. At its current state, the model clearly lacks an explicit description of a polymerization process. Thus, integrity of the modeled materials cannot be controlled, and the materials considered here (especially the higher porosity ones) do not form a self-sustained interconnected network. A more accurate depiction of the polymerization process could be developed within the kinetic Monte Carlo approach recently applied to describe polymerization processes during the formation of templated silicas.[58,59] The model can be further fine-tuned to accurately reproduce nitrogen adsorption in the microporous region. This calibration also requires the detailed experimental adsorption data in a range of MIPs at pressures below $0.01p/p_0$. To the best of our knowledge, this data is not currently available.

In the present formulation of the model, the accessibility of the porous space is not addressed. Therefore, a situation is possible where a molecule of adsorbate is inserted in a spatially isolated binding site or region of the porous structure. A more accurate description would identify the accessible regions of the porous structure (this is specific to a particular guest molecule) and allow adsorption only in those regions. Both simulation and theoretical approaches exist for this structural analysis.[60] In the context of molecularly imprinted polymers, it seems natural to incorporate both a more detailed polymerization protocol and accessibility analysis in a framework of a single model and this will be pursued in our future studies.

Experimental adsorption data indicate that MIPs are hierarchical porous materials with some microporosity present and a broad range of mesopores. It is important to realize that atomistically detailed models of MIPs will not be able to reproduce this hierarchy of pores in its full complexity. Simulation of a system featuring a single pore in a typical mesoporous range (30 nm) will require a simulation box with a side roughly six times longer than what the current model features (about 5 nm). The volume of the system will be more than 216 times the current typical volume leading to more than 200 000 interaction sites in the system. Clearly, routine analysis of these systems is impossible. Therefore, atomistic simulations are invariably limited to microporous features of MIPs.

With all these limitations, these atomistic models nevertheless open a range of very important opportunities. They provide a detailed depiction of the microporous structure, binding site heterogeneity, and adsorption and recognition processes in these structures. These models make it possible to investigate the effect of solvent presence and swelling on molecular recognition functionality. This study focuses on a very simple template (pyridine) with only one functional group, and therefore, the imprinting effects are small. Molecular recognition properties of the model are yet to be investigated (as, strictly speaking, preferential adsorption of pyridine over toluene or enhanced adsorption of pyridine in MIPs compared to NIPs cannot be viewed as molecular recognition). In the future work, we will extend this approach to more complex systems, where molecular recognition effects are expected to emerge. This preliminary study indicates that these models will play a key role in systematic design of new MIPs with tailored functionalities.

Acknowledgment. The authors thank the Engineering and Physical Sciences Research Council for the financial support through Grant EP/D074762/1 and the Edinburgh Computer and Data Facility (ECDF) for the computational facilities. The authors thank Dr. Tina Düren and Dr. Andres Mejia for useful discussions and advise.

Supporting Information Available: Additional data for the bulk EGDMA simulation, complete summary of all adsorption isotherms, details of the employed force fields and several simulation setup files. This material is available free of charge via the Internet at http://pubs.acs.org.

(58) Schumacher, C.; Seaton, N. A. *Adsorption* **2005**, *11*, 643.
(59) Schumacher, C.; Gonzalez, J.; Wright, P. A.; Seaton, N. A. *J. Phys. Chem. B* **2006**, *110*, 319.
(60) Sarkisov, L. *J. Chem. Phys.* **2008**, *128*, 044707.